A&A 472, 471–482 (2007)
DOI: 10.1051/0004-6361:20066374

Astronomy & Astrophysics

Integral-field spectroscopy of the Galactic cluster [DBS2003]8⋆,⋆⋆

Discovery of an ultra-compact HII region and its ionizing star in the bright rimmed cloud SFO49

M. Messineo[1], M. G. Petr-Gotzens[1], F. Schuller[2], K. M. Menten[2], H. J. Habing[3], M. Kissler-Patig[1], A. Modigliani[1], and J. Reunanen[3]

[1] European Southern Observatory, Karl Schwarzschild-Strasse 2, 85748 Garching bei Munchen, Germany
e-mail: mmessine@eso.org; messineo@cis.rit.edu
[2] Max-Planck-Institut für Radioastronomie, Auf dem Hügel 69, 53 121 Bonn, Germany
[3] Leiden Observatory, PO Box 9513, 2300 RA Leiden, The Netherlands

Received 10 September 2006 / Accepted 23 April 2007

ABSTRACT

Context. We have started a program of infrared (IR) studies of the stellar clusters associated with HII regions in order to understand the structure of the spiral arms and their interaction with the central bar of the Galaxy better.
Aims. This is accomplished by determining the distance to the OB stars embedded in the clusters. We want to use IR stellar spectro-photometric measurements to complement the kinematic distances from the radial velocity of the gas.
Methods. SINFONI, the infrared integral-field spectrograph of the VLT, enabled us to image the clusters and to resolve them into individual stars, to get the spectra of the brightest stars, and to analyze the possible nebular emission.
We performed pilot observations of [DBS2003]8, an embedded Galactic stellar cluster in the bright rimmed cloud SFO49, during the SINFONI science verification. The results are presented in this paper.
Results. The center of the cluster is resolved for the first time and four stars are detected, the brightest being a late O type or early B star. A spectro-photometric distance to the cluster of 2.65 ± 0.4 kpc is derived. We discovered that the O type star is located in the center of a nebula, which is quite circular in shape with an observed radius of ~0.03−0.06 pc, a value typical of an ultra-compact HII region. We measured the nebula's Br γ emission, which is generated by photo-ionization of the central star; and from the hydrogen molecular line ratio, we have proved that the ionized nebula is surrounded by a photo-dissociated region (PDR). We also detected [FeII] line emission at 1.664 μm. The ratio of the iron flux to that of the Br γ line is found 15 times higher than in a classical HII region. This suggests that at least part of the [FeII] line emission emanates from shocked stellar wind material.

Key words. stars: early-type – ISM: HII regions – Galaxy: structure – infrared: ISM – infrared: stars

1. Introduction

1.1. Embedded stellar clusters

Stellar clusters are formed continuously in the disk of a spiral galaxy, typically along the spiral arms. During the earliest stages of evolution, the clusters are completely embedded in their parental molecular clouds. The identification of embedded stellar clusters in the plane of our Galaxy and the study of their spatial distribution are therefore of primary importance for gaining a better understanding of the current star formation rate and of the Galactic structure.

Embedded clusters are good tracers of the spiral arms, but their distance determinations are difficult and often rely only on radial velocities from radio data. There is an intrinsic ambiguity when using kinematic distances inside the solar circle: each radial velocity measurement is consistent with a near and a far solution for the distance. Furthermore, it depends on the assumed model of Galactic rotation. Spectro-photometric distance estimates are not affected by the above-mentioned problems. They may actually resolve ambiguities and can provide new constraints on Galactic morphology. In the past, the necessary observations were mostly made at optical wavelengths and thus were often hampered by interstellar extinction, especially toward the central few kilo-parsecs of our Galaxy. Infrared observations can partly overcome this obstacle.

It is now possible to detect stars in highly extincted HII regions at a large distance from the Sun. Furthermore, thanks to large mid- and near-infrared surveys of the Galactic plane, such as the Two Micron All Sky Survey (2MASS), The Deep Near Infrared Survey of the Southern Sky (DENIS), the ISOGAL survey, the Mid-course Space Experiment (MSX), and the Galactic Legacy Infrared Mid-Plane Survey Extraordinaire (GLIMPSE), several hundred new Galactic HII regions and candidate infrared stellar clusters have been discovered recently, e.g. by Bica et al. (2003b,a), Dutra & Bica (2000), Dutra et al. (2003), Ivanov et al. (2002, 2005), and Borissova et al. (2003). We expect to find many new candidates for inner-Galactic clusters with the ongoing UKIDSS survey, a deeper near-infrared survey of the Galactic plane, and with future VISTA (Visible and Infrared Survey Telescope for Astronomy) surveys.

Higher-resolution infrared follow-up studies of these stellar clusters are needed in order to resolve each cluster into stars,

⋆ The acronym was given by Simbad, the CDS Database.
⋆⋆ Based on observations collected at the European Southern Observatory, Paranal Chile.

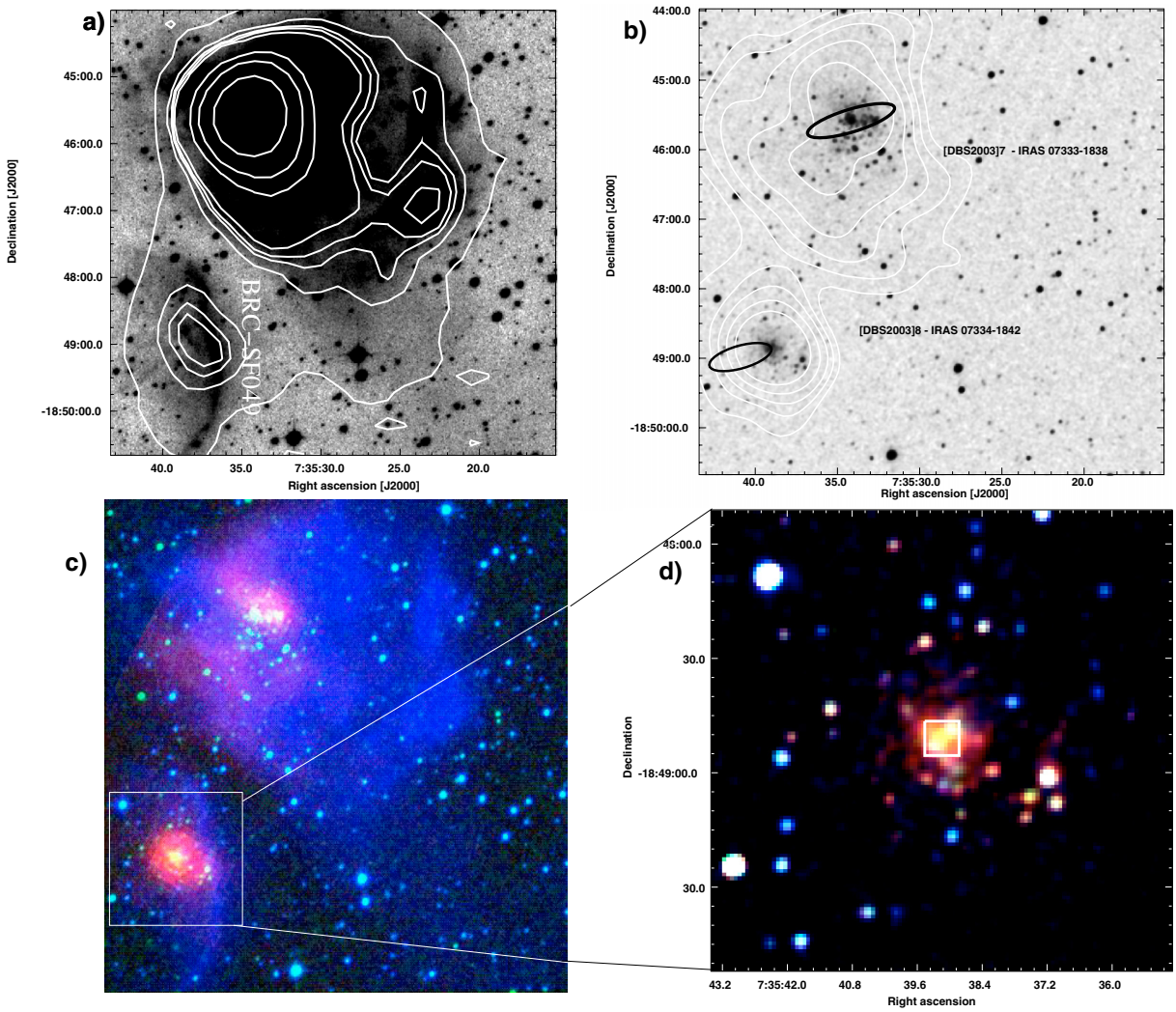

Fig. 1. Images from the *top-left* to the *bottom-right*. **a)** The gray-scale shows an Hα image taken from the SuperCOSMOS Hα survey (Parker & Phillipps 1998) in a logarithmic scale, while the contours show the NVSS 1.4 GHz radio emission of the Sh2-307 HII region. **b)** In the 2MASS K_s-band image (gray-scale) two stellar clusters are visible: at the top the cluster [DBS2003]7 and at the left-bottom the cluster here studied, [DBS2003]8. The white contours show the 8 μm emission detected with MSX. Ellipses indicate the positions of the two IRAS sources detected in the field of view, IRAS 07334-1842 and IRAS 07333-1838. The ellipses cross each axis at a positional error of 4 sigma. **c)** three-color image of the same field as in the top figures. In red the MSX A-band image, in green the 2MASS K_s-band, and in blue the Hα image. **d)** 2MASS three-color image of the area outlined in **c)**. In red the K_s-band, in green the H-band, and in blue the J-band. The square indicates the $8'' \times 8''$ field observed with SINFONI.

to understand its nature, and to estimate its photometric or spectro-photometric distance.

We have started a program with the integral-field spectrometer SINFONI (Eisenhauer et al. 2003; Bonnet et al. 2004) on ESO's Very Large Telescope to observe candidate obscured clusters in HII regions. Simultaneously recording images and spectra of early-type stars enables classification into spectral subclasses and determination of their apparent magnitudes, leading to spectro-photometric distance determinations.

1.2. Target cluster [DBS2003]8

In this paper we present near-IR observations of the stellar cluster [DBS2003]8 centered on α(J2000) = 07h35m39.3s and δ(J2000) = $-18°48'53.1''$ (l, b = 234.64°, 0.83°). The data were obtained as part of the SINFONI science verification (SV) program, during which only targets in the direction of the outer Galaxy were observable in the Chilean sky.

[DBS2003]8 is listed as a 2MASS candidate young cluster by Dutra et al. (2003). In the 2MASS images it appears as a bright unresolved source. It was selected in order to test the capability of using 2MASS data to identify candidate clusters of small angular size, which perhaps are at larger distances. Furthermore, the apparent size of the cluster's core matches the field of view of SINFONI nicely in its large field configuration.

The near-infrared cluster [DBS2003]8 is located in the direction of the HII region Sh2-307, and it is about 3.5′ away from another stellar cluster, [DBS2003]7 (Fig. 1). The HII region is clearly visible in the left-top panel of Fig. 1, where the Hα image taken from the SuperCOSMOS Hα survey (Parker & Phillipps 1998) and the NVSS 1.4 GHz radio map (Condon et al. 1998) are shown. The radio emission extends over a diameter of about 6′. The peak flux density is ∼300 mJy, and there is a secondary component to the south with a peak flux density of ∼30 mJy. The secondary radio peak coincides with the bright rimmed cloud (BRC) SFO49 (Sugitani & Ogura 1994) as traced by the Hα emission in Fig. 1.

The near-infrared stellar cluster [DBS2003]8 resides inside the bright rimmed cloud SFO49 and, as shown in the right-top panel of Fig. 1, it coincides with the mid-infrared source MSX G234.6358+00.8281, detected by the Midcourse Space Experiment (MSX) (Price et al. 2001) at a resolution of 18.3″. The mid-infrared source (IRAS 07334-1842) was also detected by the IRAS satellite, but its nominal spatial position is 29″ off from that given by MSX, probably due to confusion at the lower spatial resolution of the IRAS instruments (0.5′ at 12 μm). The flux measurements for the IRAS source are 5.98 Jy, 53.90 Jy, 234.73 Jy and <452.08 Jy at 12, 25, 60, and 100 μm, respectively, and give mid-infrared colors consistent with those of a UCHII region (Wood & Churchwell 1989a). By assuming a distance of 2.5 kpc, Sugitani & Ogura (1994) measured a far infrared luminosity $L_{\rm IR}$ of 4300 $L_{\odot}$, and predicted an embedded star of B1 spectral type (Blum et al. 2000; Panagia 1973). This cluster is then an excellent example of a newly-formed high-mass stars in a bright rimmed cloud.

Using the Australian Telescope Compact Array (ATCA), Thompson et al. (2004) mapped the radio emission around the BRC SF04 at 20 and 13 cm. The authors detected two radio sources (about 300 mJy), which do not coincide with the position of the BRC SF049 ([DBS2003]8) and are given as possible extragalactic objects. They did not detect any radio emission associated with the BRC SF049. From the NRAO VLA Sky Survey 1.4 GHz radio continuum contours (Condon et al. 1998) shown in Fig. 1, we see that the ATCA radio source SF049b clearly coincides with the stellar cluster [DBS2003]7 and that, toward [DBS2003]8, there is also an extended (80 arcsec) and weak (29 mJy) 20-cm radio source.

With the new SINFONI data we resolve the cluster [DBS2003]8 into individual stars and we are able to detect the ultra-compact HII (UCHII) region and its ionizing star. In Sect. 2 we describe the SINFONI observations and the data reduction. In Sect. 3 we present the stellar spectra, and we estimate a spectro-photometric distance to the cluster in Sect. 5. The nebular emission is discussed in Sect. 4. Final conclusions and remarks are presented in Sect. 6.

2. Observations and data reduction

Near-infrared observations in the H- and K-bands were obtained with the integral-field spectrometer SINFONI on ESO's 8.2 m telescope UT4 (Yepun) on the VLT, during the nights of 25 and 26 November, 2004, respectively. Conditions were photometric both nights, with a DIMM seeing at zenith and at 0.5 micron of 0.5−0.8″ during the first night and of 1.0″ the second.

Data were acquired using a pixel scale of 0.25″, therefore covering a field of view of 8″ × 8″, with both the H (1.45−1.85 μm) and the K (1.95−2.45 μm) grating and obtaining a typical spectral resolution of $R \equiv \lambda/\Delta\lambda = \sim$3000 in the H-band (∼5.5 Å at 1.65 μm) and $R \sim 4400$ in the K-band (∼5 Å at 2.2 μm). No guide star suited for adaptive optics (AO) was available in the vicinity of our target. We thus observed with SINFONI in the "no AO" mode. Exposures were taken in a one target-sky-sky-target sequence using a fixed sky position located 58″ east of the cluster center. The detector integration time (DIT) per individual image was 600 s and 200 s in H and K-bands, respectively, and the number of co-addings (NDIT) was 1.

Observations of a telluric standard star of spectral type G2V, HD63487, immediately followed the science observations. The integration time on the standard was 20 s and 10 s at K and H, respectively. Both the target and standard stars were observed very close to airmass 1.0.

The SINFONI field of view is dissected into 32 pieces ("slitlets") through a set of small plane mirrors with different tilt angles (image slicer). This generates a pattern that looks like a brick-wall pattern, called a pseudo-longslit. Each spatial position is then dispersed by a grating and projected onto the (2048 × 2048) pix^2 detector. For our plate scale, each slitlet is 0.25″ wide on the sky and is sampled by 64 detector pixels in the x-direction. Since each pixel is 0.125″ wide on the sky, the raw image has a spatial sampling of 0.25″ × 0.125″. The y-axis corresponds to the spectral dispersion direction.

The construction of a wavelength-calibrated 3D data cube, along with the removal of the instrumental signatures, was performed with version 1.2 of the ESO pipeline and EsoRex (Modigliani et al. 2007; Schreiber et al. 2004). Each science frame was sky-subtracted and then flat-fielded with a combined set of 6 lamp flats. Dead/hot pixels were removed by interpolation and a correction for geometric distortion was applied. A wavelength-calibration map and the wavelength-dispersion coefficients were obtained using daytime arc-lamp lines. Finally, a wavelength-calibrated data cube was generated. The wavelength dependence of the atmospheric refraction causes the apparent position of an object on the sky to change with wavelength, but the ESO pipeline
does not correct for this displacement. In the 3D data cube, this might give a drift of the object's detector position with wavelength. However the effect is negligible over the bandpass. In fact we found that the stellar centroids move less than a quarter pixel on slice images taken at the two extremes of the wavelength range in both the H and K-bands.

The coordinates of the SINFONI field agree well with the 2MASS coordinates: assuming that star A coincides with the peak intensity in the $K_{\rm s}$-band 2MASS we found an offset in absolute position of ΔRa = 0.5″ and ΔDec = 0.3″.

2.1. Photometry

The resulting H and K data cubes of the science object and of the standard star were multiplied by the 2MASS H and $K_{\rm s}$ filter response curves. Then an average image was constructed for each data cube (Fig. 2). The *FWHM*s of the objects detected in these images, all seemingly point sources, are 0.5″ and 0.6″ in the H and K-bands, respectively. As seen in Fig. 2, the K-band image looks more smeared-out than the H image, because the spatial resolution of SINFONI is actually twice as good in the x-direction as in the y-direction. While a non-integer pixel shift (jitter) was applied in the y-direction between the two on-target positions taken in the H-band, in the K-band the shift happened to be an integer number. Non-integer shifts led to a finer spatial sampling of the PSF.

The positions and photometry of the detected stars were extracted with the psf-fitting routine Starfinder (Diolaiti et al. 2000). Since this routine uses an empirical PSF, it also works well with quite elongated PSFs. As a PSF we used the median of all four brightest stars and an extraction box of 12 × 12 pixels. The extraction was performed with a detection threshold of 3 sigma and a correlation threshold of 0.90. The formal errors of the fit are within 0.05 mag, calculated by assuming a Gaussian distribution of the background noise and a Poissonian signal. For the central star, aperture photometry with the PHOT task inside IRAF was also performed in order to evaluate the psf-aperture correction and to estimate systematical photometric errors. Repeated PHOT measurements with a different background annulus and masking of the neighborhood stars gave errors within 0.1 mag. A correction of +0.17 mag was

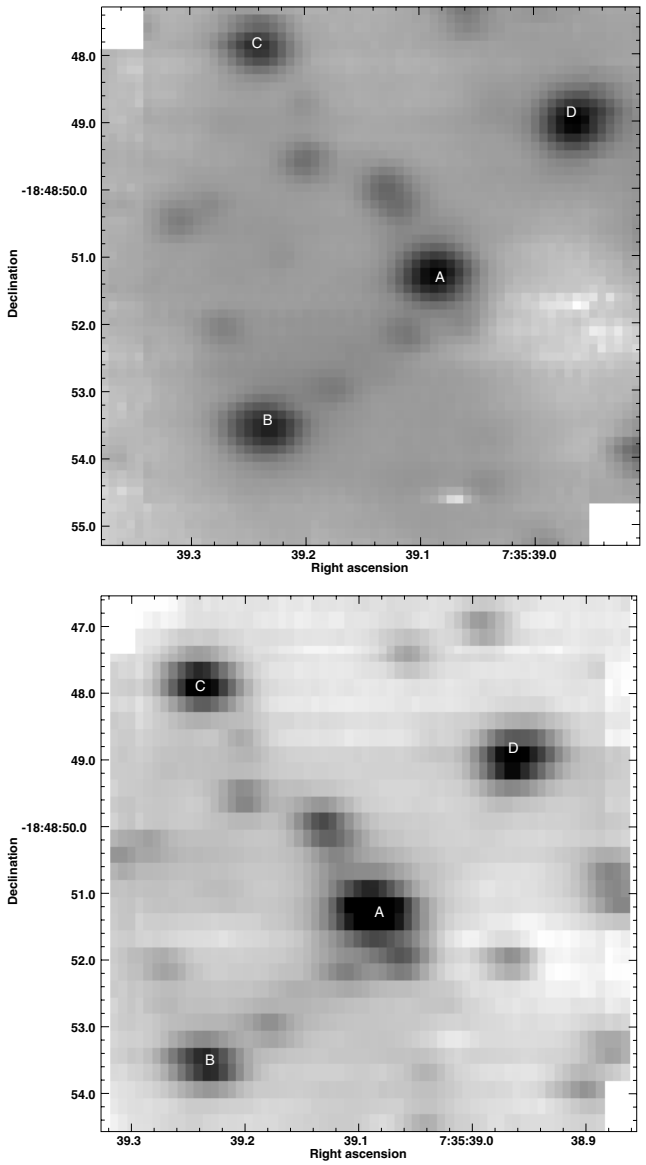

Fig. 2. SINFONI data: *Upper*: H-band average image obtained from the H-band data cube. *Lower*: K-band average image obtained from the K-band data cube. Images are shown on a logarithmic scale. The brightest objects were designated A–D.

found between the psf-fitted magnitudes and those from aperture photometry for both H and K-bands. The same correction (within 0.06 mag) is obtained for the standard star, when using the PSF extracted from the science frame.

The instrumental magnitudes were calibrated in the 2MASS photometric system using the observations of HD 63487. The respective nightly photometric zeropoints were obtained from aperture photometry applied to HD 63487, using an aperture radius of 25 pixels (3.1″). All targets and standard stars have fluxes well within the linearity range of the detector. The resulting calibrated magnitudes of the brightest objects are given in Table 1. The formal errors of the fit are within 0.05 mag; however, the absolute error is much larger (0.15 mag), as it includes systematics such as the zero point uncertainty. The estimated interstellar extinction (A_K) and stellar spectral types are listed in Cols. 4 and 5. The 2MASS magnitudes of the standard star are also reported.

Table 1. Observed magnitudes of the 4 brightest objects detected in the SINFONI field.

Star	H [mag]	K_s [mag]	A_K [mag]	Spec. type
A	14.95(±0.01)	12.93(±0.02)	3.1	O8-B1 V
B	15.56(±0.05)	14.46(±0.03)	1.2	F-G
C	15.84(±0.02)	14.19(±0.03)	1.6	K-M
D	14.94(±0.01)	13.76(±0.02)	1.4	early K
HD 63487	7.75(±0.03)	7.67(±0.02)		G2 V

2.2. Spectroscopy

The spectra of the four brightest stars (labeled A–D in Fig. 2) were extracted from the final H and K data cubes (Figs. 3 and 4). The average signal-to-noise ratio of the stellar continuum varies from 40 (star A, in both H and K-bands) to 20 (star B, in both H and K-bands).

The wavelength calibration as given by the pipeline is based on a K-band spectrum of a neon+argon lamp and an H-band spectrum of an argon+xenon lamp, taken during the same day as the observations, but during the day time, with the telescope at zenith. One can therefore expect some uncertainty in the wavelength calibration, e.g. because of mechanical flexure when observing during night at a certain elevation. We checked and corrected the wavelength calibration by using OH sky lines (Oliva & Origlia 1992; Rousselot et al. 2000). We found shifts between the solutions given by the OH lines and those given by the calibration lamp to be smaller than a quarter of pixel (0.14 Å with an rms = 0.3 Å in the K-band and of 0.4 Å with an rms = 1.0 Å in the H-band).

The average signal-to-noise ratio of the continuum of the standard star was 200 in the H-band and 250 in K-band. Hydrogen lines and metallic lines were removed from its spectrum by comparison with a high-resolution solar spectrum taken with the NSO/Kitt Peak FTS, which had been binned to the resolution of SINFONI.

In order to obtain absolute flux calibration of the data cubes, we scaled a black body spectrum with a temperature of 5636 k with the 2MASS H and K_s-band flux densities (in W cm^{-2} μ m^{-1}, Cohen et al. 2003) of the G2V standard star. Then, we divided the calibrated black body curve by the cleaned H-band and K-band spectra of the standard star (in counts/s), thus obtaining the H-band and K-band sensitivity functions. Flux-calibrated science data cubes were finally obtained by multiplying the data cube by the corresponding sensitivity function.

We used a box aperture of 3×3 pixels centered on the maximum intensity pixel (to minimize the contamination from neighboring stars and background noise). All spectra are contaminated by nebular emission (see Sect. 4), and an annular sky region surrounding the star with radius between 7 and 9 pixels and width of 1 pixel was used for subtracting both residuals of the atmospheric OH lines and nebular contamination. The remaining uncertainties in the extracted spectra, especially around Br γ, result from possible variations from point to point in both intensity and shape of the nebular emission. A visual inspection of the continuum-subtracted, two-dimensional line maps was used to confirm the presence and nature of the spectral lines, confirming that the remaining uncertainty did not affect the spectral classification.

The spectra were extracted with a fixed aperture and scaled to match the stars' 2MASS flux densities at the effective wavelength of the corresponding 2MASS filter as derived in Sect. 2.1. The factors applied were 2.4 and 4.2 for the H and

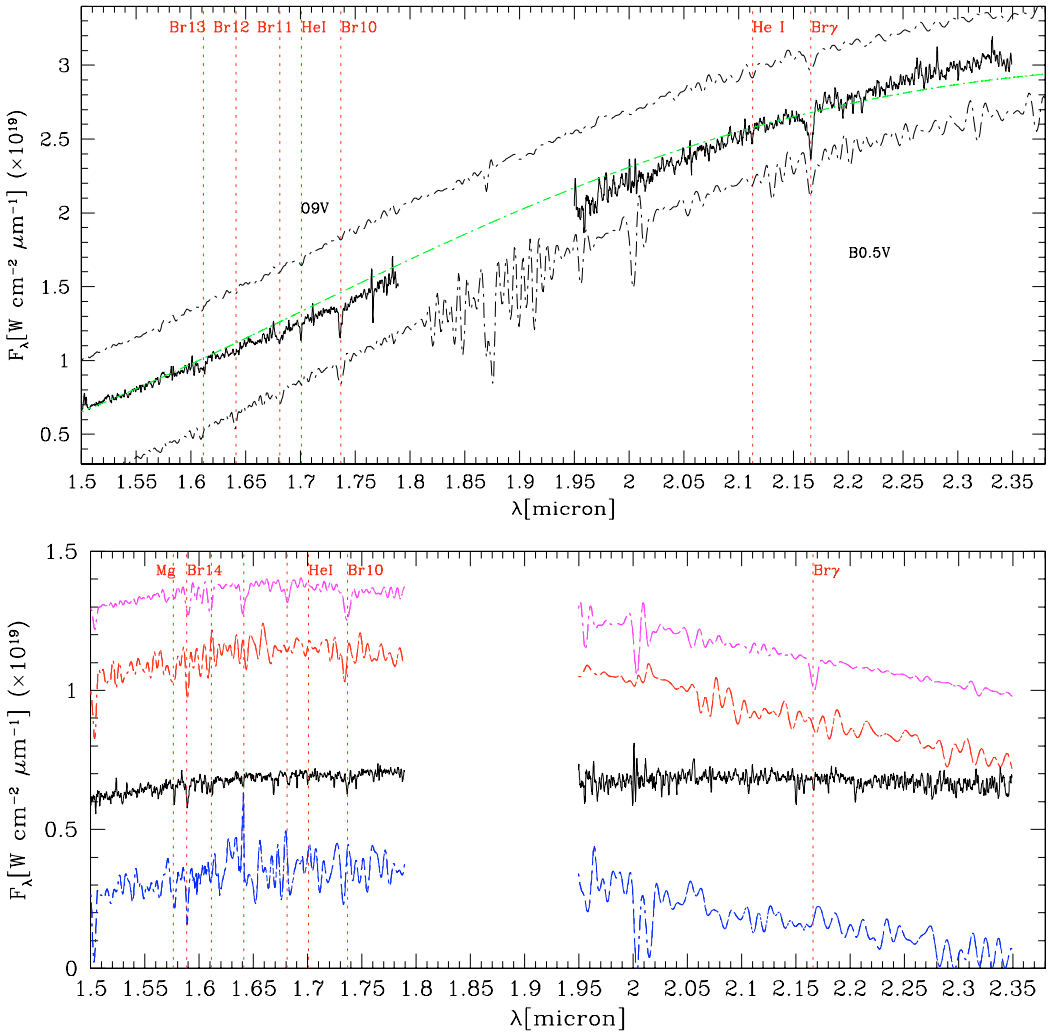

Fig. 3. *Top*: *H* and *K*-band spectrum of the central star, which is labeled with an "A" in Fig. 2. The full line shows the spectrum after correction for atmospheric absorption and instrumental response. Vertical lines indicate the location of hydrogen and helium lines (see text). The dashed curve that underlines the observed stellar spectrum is a black body with a temperature of 35 900 K and an interstellar extinction of $A_K = 3.1$ mag. For comparison, the two other dashed curves show spectra of the O9V star HR995 and of the B0.5V star HR081 (Lancon & Rocca-Volmerange 1992). These reference spectra were read as Fν vs. ν, converted to Fλ vs. λ, reddened ($A_K = 3.1$ mag), and normalized to the observed *K*-band total flux of the central star. Then for clarity an additive shift of +0.4 and −0.35, respectively, was applied. *Bottom*: spectrum of star "B" (full black line). The dashed spectra are models (Pickles 1998) for a F5, a G5, and a K3 dwarf (starting from the top) at an extinction in *K*-band of 1.2 mag. Near 2.0 micron, several telluric lines are visible due to bad subtraction of the telluric features. Vertical lines indicate the location of detected lines (see text).

K-band spectra, respectively. The integrated *H* and *K* fluxes over the corresponding 2MASS band-passes agree better than 10% and 20% with those measured from the average *H* and *K* images. The uncertainty mostly comes from the exact position of each star on its central pixel and by the somewhat degraded spatial sampling of the *K* image.

We also investigated the spectra of additional fainter sources detected in the field. However, as these objects are significantly fainter, $K > 16$ mag and $H > 18$ mag, their spectra were too noisy and no useful information could be extracted.

3. The stellar content of [DBS2003]8

We have resolved the cluster [DBS2003]8 into its individual stars for the first time. Using the Galactic differential source counts in the direction $(l, b) = (90°, 0°)$ (Wainscoat et al. 1992), one should expect to observe at most 0.2 field stars with *K* magnitudes between 13 and 15 within a field of view of $8'' \times 8''$. This value is an upper limit to the actual field contamination, since the cluster [DBS2003]8 is located at $(l, b) = (234°, 0.8°)$, i.e. toward the outer Galaxy, where the star counts predicted for an exponential disk are even lower. Therefore, it is highly likely that the four brightest stars ($K < 15$ mag) are members of the cluster.

3.1. Stellar classification

In order to perform the spectral classification, the spectra of the detected stars were compared with the *K*-band and *H*-band atlases of Blum et al. (1997), Hanson et al. (1996, 1998, 2005), Kleinmann & Hall (1986), and Meyer et al. (1998).

The *H*- and *K*-band spectra taken at the highest SINFONI resolution typically allow for a spectral classification of an early-type star within ±2 subclasses (e.g. Hanson et al. 2005). Furthermore, the use of an integral-field spectrometer enables us to simultaneously detect spectral lines from the HII region itself

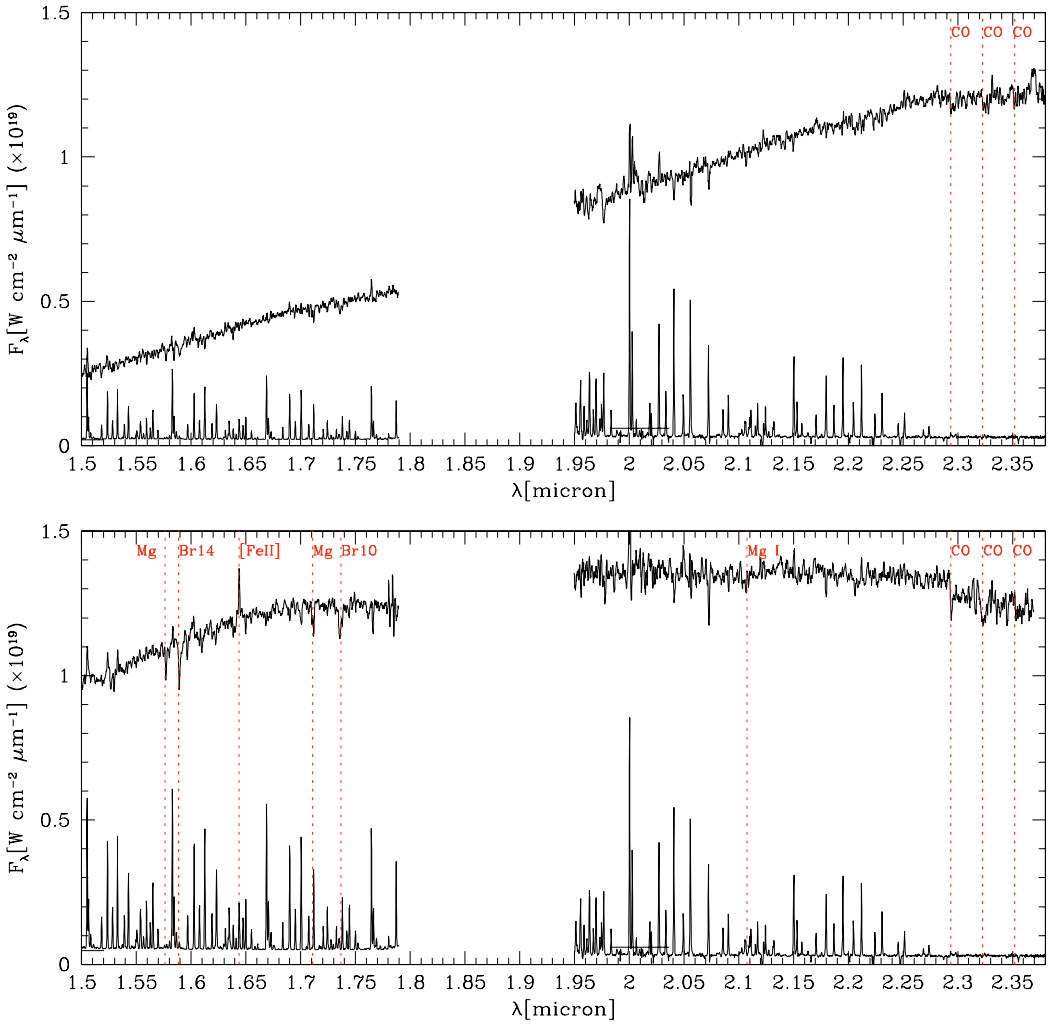

Fig. 4. *H* and *K*-band spectrum of star C (*top panel*) and star D (*bottom panel*). The strong complex of emission lines near 2.0 μm, as well as the lines at 2.0557 and 2.0723 μm, are due to a bad subtraction of telluric lines. The atmospheric OH lines are shown below each stellar spectrum for comparison.

(gas) and from the stellar sources, allowing for a proper decontamination of the stellar spectra.

3.1.1. Star A

The *H*-band spectrum of the central star, A, shows absorption lines from the Brackett series, Br10 (1.7367 μm), Br11 (1.6811 μm), Br12 (1.6412 μm), and Br13 (1.6114 μm) and the HeI line at 1.7008 μm; it does not show HeII lines. The *K* spectrum shows a strong Br γ (2.1661 μm) line, a suggestion of an HeI line at 2.1126 μm (below 2 sigma detection), and no HeII, CIV (2.078 μm), or NIII (2.1155 μm). The Br γ is clearly seen in absorption, but its equivalent width is quite uncertain (8 ± 3 Å), since it depends on the subtraction of the emission from the surrounding nebula.

By comparing the two spectra with atlases of early-type stars, we concluded that star A falls in the O9–B1 category of Hanson et al. (2005, 1998), which includes dwarf stars with optical classifications of O8, O9, B0, and some B1 stars. The luminosity class was estimated by comparison with the spectra in the Hanson et al. atlas by considering the fact that the line widths of the Brackett (Br) lines are broader in dwarf stars than in supergiants. Star A shows broad Brackett lines. We measured an *FWHM* of 21 ± 3 Å (11 pixels) and 56 ± 5 Å (23 pixels) for the Br11 and Br γ lines, respectively. Also, supergiants show the HeI lines at 2.161 μm and at 2.162 μm in the blue wing of the Br γ (Hanson et al. 2005), which at our spectral resolution would be clearly resolved (Paumard et al. 2006). Therefore we conclude that the central star is a dwarf star.

The continuum of star A has a strongly reddened appearance. We derived an estimate of the interstellar extinction toward star A by adopting an intrinsic photospheric $H - K$ color (Blum et al. 2000) and assuming that the flux in the *H* and *K* bands is photospheric, i.e. that there is no excess due to an accretion disk. We further adopted an infrared extinction power law with an index of 1.9 (Messineo et al. 2005). The deduced value of interstellar extinction corresponds to an absorption of $A_{\rm K} = 3.10 \pm 0.26$ mag and is independent of the stellar sub-types used for star A due to the infrared color degeneracy within the considered stellar sub-types.

Figure 3 shows the observed spectrum of star A plotted with a black body of temperature 35 900 K and interstellar extinction $A_{\rm K} = 3.1$ mag, along with the observed spectra of the O9V star HR995 and of the B0.5V star HR081 (Lancon & Rocca-Volmerange 1992) for comparison. Lancon's spectra were read as F_ν vs. ν, converted to F_λ vs. λ, reddened to $A_{\rm K} = 3.1$ mag and normalized to the observed *K*-band total flux

Table 2. Detected nebular emission lines.

Line	λ	*FWHM*	Peak_{tot}	$\text{Continuum}_{\text{tot}}$	rms_{tot}	Flux_{tot}	Flux_{30}
	[μm]	[Å]	[10^{18} W cm^{-2} μm^{-1}]	[10^{18} W cm^{-2} μm^{-1}]	[10^{18} W cm^{-2} μm^{-1}]	[10^{22} W cm^{-2}]	[10^{22} W cm^{-2}]
[FeII]	1.64400	7.2	2.21	1.02	0.06	8	6
H_2 1-0 S(1)	2.12183	6.2	4.69	0.99	0.06	23	16
Br γ	2.16612	6.5	3.03	1.11	0.03	13	11
H_2 1-0 S(0)	2.22329	5.7	3.12	1.17	0.03	12	8
H_2 2-1 S(1)	2.24772	6.6	2.97	1.19	0.03	11	8

of the central star. The slope of the spectrum of star A agrees quite well with that of the comparison stars (within 6%). This implies a negligible K-band excess and implies that there is no disk emission around star A. The star has mostly likely completed its accretion phase.

3.1.2. Star B

The detection of Mg(1.576 μm) and HI (Br14 at 1.5885 and Br10 at 1.7367 μm) lines suggests that star B has a spectral type between late F and early G types. Fitting the observed H-band spectrum with a G5V model spectrum from Pickles (1998), extincted by $A_{\rm K} = 1.2 \pm 0.1$ mag, gives a reasonable agreement. However, the flat slope observed in the K-band indicates an infrared excess (up to 30%), which is probably explained by the star B being a young stellar object with circumstellar emission. The K-band excess is well-fitted by adding a second black body component with a temperature of 600 K. Assuming a cluster distance of 2.5 kpc (Sect. 4) and an interstellar extinction of $A_{\rm K} = 1.2$ mag, the resulting absolute K magnitude of star B is ~1.3, consistent with a ~2 $M_\odot$ pre-main-sequence star. The observed dereddened $H - K$ color of 0.34 mag is indeed much redder than the expected intrinsic color for G dwarfs (~0.05−0.06 mag, Bessell & Brett 1988), but it is within the observed range of dereddened colors of classical T Tauri stars (e.g. Eiroa et al. 2001; Meyer et al. 1997).

The interstellar extinction derived from our spectrum of star B is much lower than that measured towards the central star of the cluster. If we implicitly assume that the extinction is constant throughout the nebula, this suggests that star B is located in front of the nebula that surrounds star A. However, it could very well be that the extinction intrinsically peaks strongly on star A.

3.1.3. Star C

The H-band spectrum of object C is quite noisy and featureless. In the K-band, absorption from ^{12}CO band heads is clearly visible, which indicates that object C is a cool, late-type star. Other absorption lines featuring a K-band spectrum of cool stars are from NaI and CaI. Typically the strengths of the two atomic lines in spectra of dwarf stars is half that of the CO band head (Kleinmann & Hall 1986). Since we detected CO band-head absorption with a signal-to-noise of only about four, we expected the NaI and CaI lines to be below a signal-to-noise of two. The red $H-K$ color (1.65 mag) and the lack of other identifiable photospheric lines suggest that star C is another young stellar object. Assuming a typical color of $H - K = 0.6$ mag, which is an average color between the end of the classical T Tauri star locus ($H - K = 1.0$ mag) and the average intrinsic color for late type dwarfs ($H - K = 0.2$ mag) (Meyer et al. 1997; Eiroa et al. 2001; Bessell & Brett 1988) would yield an extinction of $A_{\rm K} = 1.6$ and an absolute K magnitude of about 0.6 mag at a distance of 2.5 kpc.

3.1.4. Star D

We detected photospheric Mg, HI and CO lines, which point to an early K star. Iron emission from the ionized nebula is visible in the stellar spectrum and discussed in Sect. 4.

An interstellar extinction of about $A_{\rm K} = 1.4$ mag (and therefore a dereddened color of $H - K = 0.24$ mag) is needed in order to fit the H-band continuum of a late dwarf (Pickles 1998). By assuming a distance of 2.5 kpc (Sect. 5), we derive an absolute K of 0.4 mag. An intrinsic redder color of $H - K = 0.6$ mag would yield $A_{\rm K} = 0.9$ mag and absolute $K = 0.9$. Because star D appears to have a lower interstellar extinction than star A, it might be located in front of the nebula, and it cannot be a background K giant star (a K giant star would yield a distance of about 5 kpc). We therefore believe it is another pre-main sequence star related to the young cluster. A foreground early main-sequence star (intrinsic $H = 4.19$ and $K = 4.08$ mag, from Wainscoat et al. 1992) would require an extinction of $A_{\rm K} = 1.6$ mag and a distance of only 400 pc.

3.2. Other stars

Several fainter stars are visible in the average H and K data cubes. Their spectra were very noisy. Their photometry was also uncertain because of crowding and because some of them are detected at the edge of the array. Their average $H - K$ color was 1.7 mag and their H magnitude was fainter than 18. At the cluster's distance this color and magnitude could correspond to stars similar to star B, C, or D, if at higher extinction ($A_{\rm K} = 2.5$). Several of these stars could therefore be associated with the HII region Sh2-307 and be located behind the nebula.

4. Nebular emission

The SINFONI data reveal the presence of a nebula that surrounds the central star (Fig. 7). Nebular emission lines from molecular hydrogen, ionized hydrogen, and singly ionized iron were detected (Table 2 and Fig. 5). No shifts in wavelength (and therefore in velocity) of the lines were detected with spatial position. The detected lines appear to be barely resolved in our SINFONI data.

The Table 2 reports the name of the detected line and its characteristics over the whole field of view: *FWHM* of the line, the peak intensity (including the continuum), the intensity of the adjacent continuum and the standard deviation of the continuum. Two integrated fluxes are listed; the first is the integrated flux over the whole field of view, while the second is the flux over a circular area with a radius of 3.75″ (30 pixels) centered on the central star. This circle encloses the region where most of the Br γ emission is located, while the molecular hydrogen is

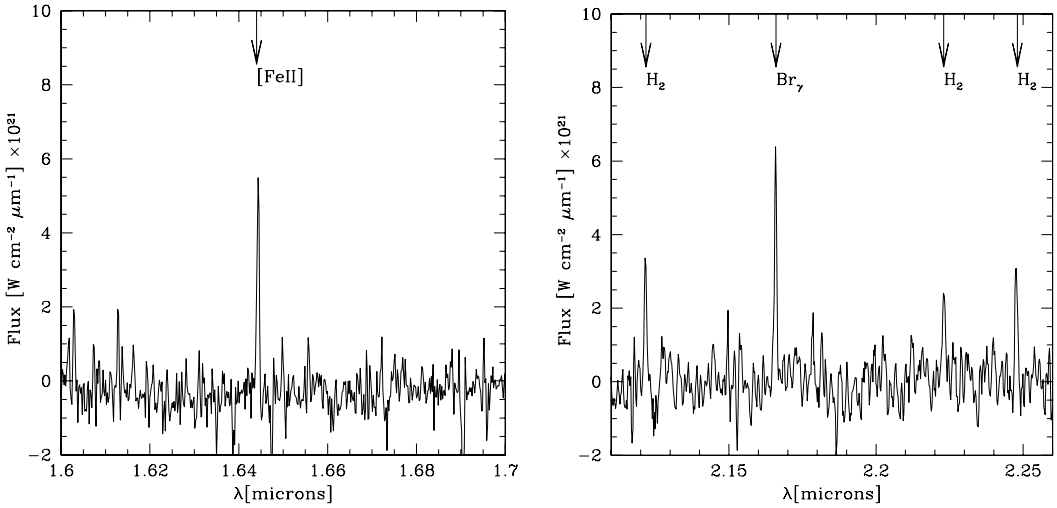

Fig. 5. Example of the nebular spectrum. To remove the sky line residuals we plotted the difference between two spectra extracted at two different positions of the nebula: one spectrum is taken from the peak of emission of the Br γ and integrated over an area of $0.375'' \times 0.375''$; the other spectrum is taken in a region of the lowest intensity of the Br γ. *Left*: *H*-band spectrum *right*: *K*-band spectrum

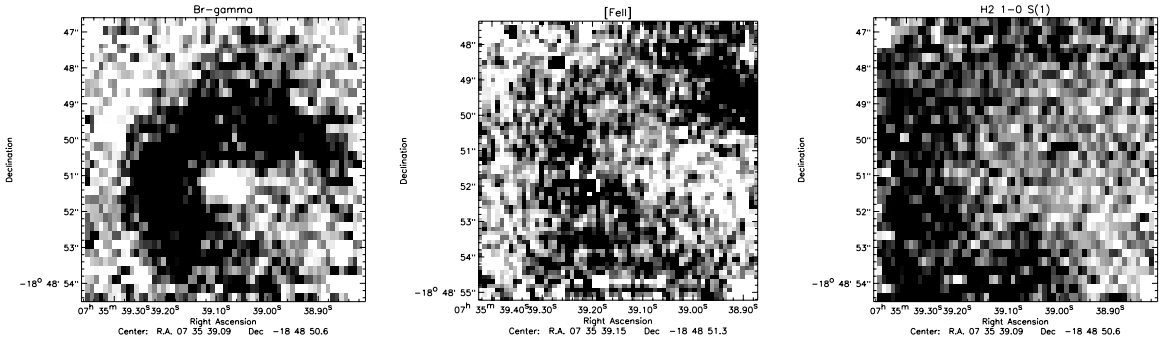

Fig. 6. Maps of the Br γ, FeII and H2 emission. The maps are obtained integrating in wavelength over a range centered on the line and 3 times the line's *FWHM* broad. The continuum has been subtracted.

spread out more. The integrated fluxes were obtained by fitting the line with a Gaussian model, and their uncertainty can be up to 10% due to adjacent sky line residuals.

4.1. Ionized hydrogen and radio emission

Figures 6 and 7 show the relative location of the molecular and ionized hydrogen emission. The Br γ emission appears as a circle with a radius of about 30 pixels (3.75″). The intensity of the gas appears significantly lower (4σ) on the south west side of the nebula on both the ionized and molecular hydrogen emission maps. This same spatial gradient in the nebular emission is found when reducing the data with a different sky position and is therefore not an artifact generated by subtracting a sky that contains a positive feature. It could be due to a higher interstellar extinction on that side of the nebula. Evidence for this comes from the fact that there is a very red object at this position (seen only in the *K*-band). Unfortunately, it is not possible with the present data to generate an extinction map. A high-resolution radio continuum map would be needed in combination with the Br γ data.

With a spectro-photometric distance of about 2−3 kpc and from the observed angular size, we derive a linear radius of 7400−11 000 AU (0.036−0.054 pc) for the ionized nebula, which is a typical size for a UCHII region (Wood & Churchwell 1989b).

Given the estimate of the Lyman continuum photons N(LyC) from the central star, one would expect radio emission from a UCHII region (Panagia 1973), but only a faint (29 mJy at 1.4 GHz) and extended ($80'' \times 36''$) radio emission has been detected so far at the position of [DBS2003]8. However, the radio emission from such a UCHII region could have a very weak flux density and be "buried" under the observed extended emission.

Indeed after computations and in the simplest possible model of a photoionized nebula in which a single massive star is in a uniform cloud of hydrogen, we found that the radio emission is expected to be very low. Since in a Strömgren sphere, a sphere with a radius at which the stellar photon output rate just balances the recombination rate, both the free-free emission and the estimate of the N(LyC) are proportional to the square of the electron density (n_e) times the volume of the nebula. It follows that the integrated free-free emission from a Strömgren sphere is independent of its size or density and only depends on the N(LyC) from the star. Inverting Eq. (5.5) in Martín-Hernández et al. (2003), we expect radio continuum flux densities for O9, B05, and B1 dwarf stars at a distance of 2.5 kpc at 1.4 GHz of 3.65, 0.05, 0.006 Jy, respectively. By comparing these values with the observed 1.4 GHz radio flux at the position of [DBS2003]8, one concludes that a later type, B0.5-B1, dwarf star would give a lower estimate for the free-free radio emission and therefore consistency with the radio observations.

However, if dust absorption and free-free self absorption are not negligible, then there would be less free-free emission coming out of the HII region than what is expected from the

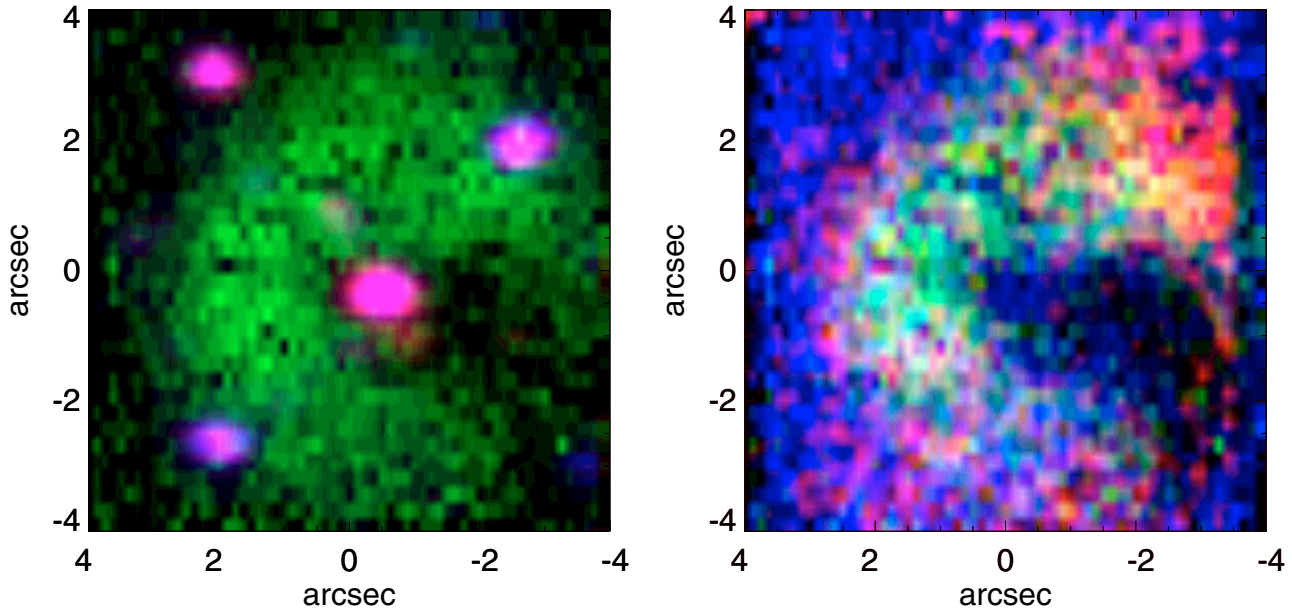

Fig. 7. *Left*: three-color image of the Galactic stellar cluster [DBS2003]-8. In blue the *H*-band image is shown, in green the Br γ image, and in red the *K*-band image. The central star appears surrounded by a nebula. *Right*: three-color image of the nebula: in blue the map of H_2 at 2.12 μm, in green that of the Br γ emission and in red that of [FeII] at 1.644 μm.

NLyc of the central star in an optically thin Strömgren sphere. Assuming a temperature, T_e, of about 10 000 K and the radius of the Br γ emission, one can estimate the electron density (n_e): $(1.5–3)\times10^4$ cm^{-3}, $(3–6)\times10^3$ cm^{-3}, if the central star is an O9V or a B0.5V star, respectively. The fluxes of Lyman continuum photons (N(LyC)) for the dwarf stars are taken from Panagia (1973). Using the size of the nebula in the Br γ line and the estimated value of n_e, we calculated the emission measure EM and therefore the optical path length for free free emission τ_ν:

$$EM = n_e^2 \times \mathrm{diameter[pc\ \ cm^{-6}]},$$

$$\tau_\nu = 8.235 \times 10^{-2} \times EM \times T_e[\mathrm{K}]^{-1.35} \times \nu[\ \mathrm{GHz}]^{-2.1}.$$

We derived an optical depth at 1.4 GHz, $\tau_{1.4\ \mathrm{GHz}}$, of about 8.5 and 0.1 for an O9V and a B05 star, respectively. Free-free self absorption is indeed important if the central star is an O9V star. Therefore the low radio flux does not rule out the central star being type O9V.

4.2. Molecular hydrogen

The mean ratio of the H_2 1-0 S(1) and H_2 2-1 S(1) fluxes integrated over the whole field is 1.9. This ratio is similar to what has been measured towards the Orion bar and Orion S regions (Luhman et al. 1998). A value of about 2 would be expected for fluorescent emission (Black & van Dishoeck 1987), and a value of about 10 if the emission is collisionally excited (Scoville et al. 1982). This indicates that our nebula is surrounded by a photodissociation region (PDR).

4.3. Iron emission

We detected [FeII] nebular emission at 1.644 μm. The iron emission is extended, and its spatial distribution follows that of the ionized gas quite well. However, it seems to extend farther out from the central star than the Br γ emission, and its intensity is stronger at the edge of the HII region, probably tracing the ionization front. The mean ratio over the entire nebula of the [FeII] and Br γ flux is 0.6, varying radially from 0.3 at the center to about 1.5 at the edge of the ionized nebula.

The FeII emission is a tracer of partially ionized regions and ionization fronts. In particular, infrared [FeII] emission is a tracer of dense regions and/or fast shocks. The iron abundance is very low, in standard HII regions and PDRs. In the Orion bar and Orion S regions, the flux of the [FeII] line at 1.64 μm is 0.1 times that of the Br γ (Luhman et al. 1998). We have derived a ratio 15 times higher than the ratio measured in the Orion bar. In shock-excited regions such as supernova remnants, this ratio is generally above unity. For example, in the supernova remnant IC443, Graham et al. (1987) find that the flux of the [FeII] at 1.64 μm emission is 30 times that of the Br γ emission. Therefore, the measured ratio suggests a more efficient excitation of FeII or an overabundance of gaseous iron which could be due to destruction of dust grains in a shocked region.

4.4. Extinction

The interstellar extinction can be estimated by comparing the observed and predicted Br γ flux. In a Strömgren sphere, there is a clear relation between the Br γ flux ($F_{\mathrm{Br}\gamma}$) and the optically thin radio free-free emission (e.g. Lumsden & Puxley 1996):

$$F_{\mathrm{Br}\gamma} = 2.45 \times 10^9 \times S_\nu \times \nu^{0.1} \times (T_e/10\,000)^{0.35} \times j_{\mathrm{Br}\gamma}[\mathrm{W\ cm^{-2}}].$$

If we assume a flux density $S_\nu = 0.029$ Jy at a frequency $\nu = 1.4$ GHz, an electron temperature $T_e = 10\,000$ k, and an emissivity $j_{\mathrm{Br}\gamma} = 3.41 \times 10^{-28}$ W m^{-3} (Storey & Hummer 1995, $n_e = 10^4$ cm^{-3}, case B), we derive an upper limit for the Br γ flux of 2.51×10^{-20} W cm^{-2}. By comparison with the observed Br γ flux of 1.3×10^{-21} W cm^{-2}, we calculate an optical depth at 2.16 μm, $\tau_{2.16}$, of 2.9. This value is in good agreement with the *K*-band extinction we derived for the central star.

Similarly, one can compare the observed Br γ flux with what is predicted for a Strömgren sphere with a given *NLyc* (s^{-1}) and at a given distance ($d = 2.5$ kpc):

$$F_{\mathrm{Br}\gamma}[10^{12}\ \mathrm{erg\ s^{-1}\ cm^{-2}}] = 0.1149 \times 10^{-45} \times d^{-2} \times NLyc.$$

Table 3. Estimates of distance modulus (DM) and distance (d) to the central star by assuming possible spectral sub-classes.

Sp.	mag K	$H-K$	A_{K_s}	DM	σ(DM)	d [kpc]	$\sigma(d)$ [kpc]
O9	−2.62	−0.05	3.11	12.44	0.3	3.08	0.46
B0	−2.36	−0.05	3.11	12.18	0.3	2.74	0.41
B0.5	−2.28	−0.04	3.09	12.12	0.3	2.65	0.39
B1	−0.94	−0.04	3.09	10.78	0.3	1.43	0.21

For O9, B0.5, and B1 dwarf stars, we derive a $\tau_{2.16}$ of 7.5, 3.5, 1.1, respectively. The assumption of a B0.5 star gives a good match with the extinction derived from our spectro-photometry of the central star A (see Sect. 2.1).

5. Distance

We derive a geocentric distance to star A using our spectro-photometric measurements, the absolute H and K magnitudes from Blum et al. (2000) and the near-infrared extinction law given by Messineo et al. (2005).

Blum et al. (2000) derived absolute K magnitudes for zero age main-sequence early-type stars using the models of Schaller et al. (1992), the relationships between temperature and spectral type, and temperature and visual bolometric correction from Vacca et al. (1996), and $V-K$ colors from Koornneef (1983).

In Table 3 we list the determinations of spectro-photometric distances for each possible stellar sub-type and constrain an average distance value to star A of 2.5 ± 0.7 kpc. The error on the distance is dominated by the uncertainty on the spectral type. The major uncertainty in the distance determination is due to the lack of precise knowledge of the spectral type. Absolute magnitudes are taken from Blum et al. (2000). The tabulated values give an average distance of 2.5 ± 0.7 kpc.

There are systematics that we need to consider for a correct estimate of the bolometric magnitudes of early-type stars, hence of their distances. The evolution of early-type stars is complicated by the presence of stellar winds and mass loss that influence the lifetime and the accretion history of the star. A new consistent set of infrared absolute magnitudes and bolometric corrections has been recently published by Martins & Plez (2006). These authors show that an increase in the mass loss rate from $1.32\times10^{-5}\ M_{\odot}\,\mathrm{yr}^{-1}$ to a value that is three times larger would change the absolute K magnitude by 0.2. A comparison between the absolute magnitudes given by Blum et al. (2000) and those from Martins & Plez (2006) shows that current models for a given temperature predict consistent bolometric magnitudes within 0.1 mag. However, the models by Martins & Plez (2006) give lower temperatures than those given by Blum et al. (2000) by a few thousand Kelvin for a given spectral type. Finally, there is a difference of about 0.8 mag for late O types between the ZAMS and the "normal" main-sequence (Martins & Plez 2006). The assumption of a main-sequence star rather than a zero age main-sequence (ZAMS) star would shift the average distance of star A to 3.5 ± 1.3 kpc.

Since star A is still embedded in its cocoon and in the early stage of forming a UCHII region (see Sect. 4), we assume the distance derived for a ZAMS star by using the calibration of Blum et al. (2000). Furthermore, by adding the considerations on the nebular extinction (Sect. 4.4), we can narrow the range of spectral type of star A to that of a B0.5 and, therefore, adopt a distance of 2.65 ± 0.4 kpc.

Table 4. Estimates of the distance to the HII region Sh2-307 from the literature.

Distance [kpc]	Reference	Comments
4.2	Russeil et al. (1995)	kinematic
3.08 ± 0.7	Brand & Blitz (1993)	kinematic
2.45 ± 0.36	Georgelin et al. (1973)	kinematic
2.2	Hunter & Massey (1990)	kinematic
2.2	Moffat et al. (1979)	*UBV* photometry
3.6	Russeil et al. (1995)	*UBV* photometry

Table 5. Measured radial velocities.

Line	$v_{\rm LSR}$ [km s^{-1}]
Br γ	49 ± 3
H_2 1-0 S(1)	43 ± 6
H_2 1-0 S(0)	42 ± 3
H_2 2-1 S(1)	46 ± 3
[FeII]	53 ± 3

In Table 4 we report kinematic and photometric distances to Sh2-307 indicating the corresponding reference. Our determination of the distance to [DBS2003]8 falls within the range of previous kinematic determinations. There is also a good match with previous optical photometric distances to OB stars in the field of Sh2-307. This confirms that [DBS2003]8 is physically associated with the Sh2-307 HII region.

From CO and Hα measurements (Russeil et al. 1995), the HII region Sh2-307 appears to have a radial velocity $v_{\rm LSR}$ of 46.2 ± 0.6 km s^{-1} (*FWHM* of 2.4 km s^{-1}) or 37 km s^{-1} (*FWHM* of 30 km s^{-1}), respectively. The authors find that the profile of the Hα line is well-fitted by two Gaussian curves with velocities of 44 and 32 km s^{-1}. With a half-power beam-width of 60″, Shepherd & Churchwell (1996) detected ^{12}CO ($J=1-0$) at a velocity of $v_{\rm LSR}=+47.0$ km s^{-1} (*FWHM* of 3.7 km s^{-1}) at the nominal position of the IRAS 07334-1842 point source (α(J2000) = 07:35:41.0, δ(J2000) = −18:48:59.0), i.e. only 24″ away from the center of the cluster [DBS2003]8.

We obtained radial velocity measurements by means of a Gaussian fit to the detected molecular hydrogen emission lines and to the nebular Br γ emission line (see Table 5) and derived an average velocity $v_{\rm LSR}=46.4\pm0.9$ km s^{-1} with an rms of 4.5 km s^{-1}. The wavelengths of the detected lines were calibrated against a few nearby OH sky lines and have an accuracy of about 4 km s^{-1} in K-band and 7 km s^{-1} in H-band. Within the errors, the measured radial velocity of the near-infrared nebula detected with our SINFONI data is consistent with that of the HII region Sh2-307. This evidence proves the physical association between the HII region Sh2-307 and the cluster [DBS2003]8.

6. Remarks on spectro-photometric distances

The uncertainty on the spectro-photometric distance is dominated by the uncertainty in the determination of the spectral type. In the case of cluster [DBS2003]8, for example, the ambiguity between spectral types O9–B1 results in a distance modulus uncertainty of about 1.6 mag. While for [DBS2003]8 this translates into an uncertainty in distance of about one kiloparsec, it would translate into a range of possible distances from 3.8 to 16.5 kpc at the distance of the Galactic center (DM = 14.5 mag). Therefore, spectro-photometric distances of individual stars farther away from the Sun than a few kiloparsecs are not much help

for Galactic studies. However, the accuracy can be notably improved with better statistics, i.e. when considering clusters with several OB stars of different spectral types. In a forthcoming paper we will also discuss spectro-photometric distances of several other embedded stellar clusters.

Improvements in the determination of distances will be the natural outcome of the recent progress in modeling infrared photospheric lines. By fitting infrared spectral lines taken at high resolution (5000−8000) and with a signal-to-noise of at least 100, one can directly estimate temperatures and gravity for individual OB stars (Repolust et al. 2005). High-quality near-infrared spectra of many OB stars must be obtained and supplied to fine-tune the theoretical modeling, while improved techniques of model fitting applied to these spectra will finally lead to the precision in distance determination that is required to constrain the inner Galactic structure.

The combination of several wavelengths and the simultaneous considerations on the energetics of the gas surrounding the early-type stars and the stellar energetics allow the possible range of spectral type and therefore the distance estimates to be narrowed down even more.

7. Summary and conclusion

New data of the Galactic cluster [DBS2003]8 obtained with the ESO near-infrared integral-field spectrograph SINFONI have been presented. For the first time the observations resolve this cluster into several stellar objects, of which the four brightest were investigated in detail using spectro-photometric measurements.

The K-band brightest star, which is located in the cluster center, presents the spectral lines typical of a late O or early B type dwarf star and is surrounded by an almost entirely spherical ionized nebula. There is no evidence of a significant excess in K-band, suggesting that the star is no longer accreting. The three other bright sources have later spectral types (later than F) and show signatures of excess emission in the K-band, which probably arises from circumstellar accretion. We thus conclude that these stars are very likely moderately massive or low-mass young stellar objects.

We then derive the first spectro-photometric distance to the cluster of 2.5 ± 0.7 kpc by assuming the central source is a zero-age main−sequence star with spectral type between O9 and B1. From a consistency check between the stellar spectral type and the observed nebular Br γ and radio continuum fluxes, we prefer a B0.5V star and, therefore, a distance of 2.65 ± 0.35 kpc. This distance is compatible with that of Sh2-307. Furthermore, by fitting the nebular lines, we obtain an average radial velocity measurement $v_{\rm LSR} = 46.4 \pm 0.9$ km s^{-1}, which is also consistent with the radial velocity of the HII region Sh2-307. Therefore we conclude that the cluster belongs to the HII region.

Our SINFONI data further led to the detection of a compact ionized nebula, which shows several characteristics of a UCHII region. Considering the simple assumption of a spherical and homogeneous nebula, we derived a linear nebular radius of 0.03−0.06 pc, which is typical of a UCHII region. IRAS measurements and colors agree with the Wood & Churchwell criteria for UCHII regions and confirm the presence of a hot dust cocoon. However, only a faint extended source was observed at the position of the nebula at radio wavelengths. On the other hand, we estimate that the radio continuum free-free emission of the UCHII region is expected to be low and therefore should be buried in the 29 mJy extended NVSS radio emission detected at the position of the cluster [DBS2003]8. Our analysis of strong molecular hydrogen emission lines, also detected from the nebula, indicates fluorescent excitation and shows that the UCHII region is surrounded by a photo-dissociation region (PDR). The flux of the [FeII] line at 1.644 μm expressed as a fraction of the Br γ line is, however, up to 15 times larger than that of the well-studied proto-type PDR of the Orion bar. The presence of [FeII] suggests the presence of a shock at the ionization front, perhaps due to a collision of the stellar winds with the molecular cloud. There is also the possibility of a circumstellar outflow interacting with the surrounding cloud. However, a simple gradient in the nebular density of an HII region could also produce a shocked ionized front.

In order to establish the nature and conditions of the nebula more precisely, its excitation mechanism, and the relative importance of photo-ionized region versus a possible outflow, follow-up studies are needed. Radio recombination-line and radio-continuum measurements, e.g. with the VLA or the ATCA, would yield a measure of the electron temperature and a better estimate of the electron density. Radio observations in combination with infrared ionized hydrogen lines (Br γ, Brα, Pfγ) would yield a proper study of the nebular optical depth (Simon et al. 1983). Deeper higher-resolution near-infrared line observations (at J- and H-band) to detect several iron transitions would yield measurements of the density and velocity of the gas at the front shock.

An additional important result of this paper is the identification of star A as the ionizing star of the UCHII region in [DBS2003]8. The detection of the ionizing source of a UCHII region is often difficult, because high interstellar extinction and veiling from the dust cocoon hamper the detection of the embedded star even in the near-infrared (e.g. Hanson et al. 2002). This newly discovered object represents a good laboratory for studying and testing the evolutionary theory of early-type stars and the interplay of their radiation with the surrounding interstellar medium. Interestingly, stars B, C, and D are all at a same (projected) distance from star A, and all near the edge of the Br γ emission. This seems to suggest a small-scale sequential star formation that is induced by the expansion of the ionizing front of the UCHII region into the molecular cloud and by the consequent shocks into the molecular gas. Young stellar objects at the border of an expanding UCHII region in a BRC have already been observed elsewhere, e.g. in RCW 108 Urquhart et al. (2004).

The whole region around the cluster [DBS2003]8 deserves further study. If the two clusters were associated with the same HII region, [DBS2003]7 would have been formed first and triggered the collapse of [DBS2003]8 via a radiative-driven implosion mechanism. In fact, [DBS2003]8 is located in the bright-rimmed cloud SFO49 discovered by Sugitani & Ogura (1994), and the curvature of the BRC suggests that the UV ionizing flux causing the implosion could be associated with the adjacent cluster [DBS2003]7. Sequential star formation has already been observed in several BRCs around HII regions Sugitani et al. (e.g. 1995).

Follow-up infrared observations of the entire area to include cluster [DBS2003]7 are required for studying the stellar population, the initial mass function, and age of both clusters and of the surrounding field. In the radio regime, ^{12}CO line mapping would yield the velocity field and therefore a better understanding of the connection between the two clusters.

Acknowledgements. We thank all members of the SINFONI SV team for having accepted our proposal. Observations could not have been carried out without the help of Sabine Mengel, Thomas Szeifert, and Christophe Dumas.

M.M. is grateful to Frank Bertoldi for useful discussion of the nebula, and to Melanie Johnston-Hollitt and Michelle Doherty for their careful reading of the manuscript. NSO/Kitt Peak FTS data used here were produced by NSF/NOAO.

References

Bessell, M. S., & Brett, J. M. 1988, PASP, 100, 1134
Bica, E., Dutra, C. M., & Barbuy, B. 2003a, A&A, 397, 177
Bica, E., Dutra, C. M., Soares, J., & Barbuy, B. 2003b, A&A, 404, 223
Black, J. H., & van Dishoeck, E. F. 1987, ApJ, 322, 412
Blum, R. D., Ramond, T. M., Conti, P. S., Figer, D. F., & Sellgren, K. 1997, AJ, 113, 1855
Blum, R. D., Conti, P. S., & Damineli, A. 2000, AJ, 119, 1860
Bonnet, H., Abuter, R., Baker, A., et al. 2004, The Messenger, 117, 17
Borissova, J., Pessev, P., Ivanov, V. D., et al. 2003, A&A, 411, 83
Brand, J., & Blitz, L. 1993, A&A, 275, 67
Cohen, M., Wheaton, W. A., & Megeath, S. T. 2003, AJ, 126, 1090
Condon, J. J., Cotton, W. D., Greisen, E. W., et al. 1998, AJ, 115, 1693
Diolaiti, E., Bendinelli, O., Bonaccini, D., et al. 2000, A&AS, 147, 335
Dutra, C. M., & Bica, E. 2000, A&A, 359, L9
Dutra, C. M., Bica, E., Soares, J., & Barbuy, B. 2003, A&A, 400, 533
Eiroa, C., Garzón, F., Alberdi, A., et al. 2001, A&A, 365, 110
Eisenhauer, F., Abuter, R., Bickert, K., et al. 2003, in Instrument Design and Performance for Optical/Infrared Ground-based Telescopes, ed. M. Iye, & A. F. M. Moorwood, Proc. SPIE, 4841, 1548,
Georgelin, Y. M., Georgelin, Y. P., & Roux, S. 1973, A&A, 25, 337
Graham, J. R., Wright, G. S., & Longmore, A. J. 1987, ApJ, 313, 847
Hanson, M. M., Conti, P. S., & Rieke, M. J. 1996, ApJS, 107, 281
Hanson, M. M., Rieke, G. H., & Luhman, K. L. 1998, AJ, 116, 1915
Hanson, M. M., Luhman, K. L., & Rieke, G. H. 2002, ApJS, 138, 35
Hanson, M. M., Kudritzki, R.-P., Kenworthy, M. A., Puls, J., & Tokunaga, A. T. 2005, ApJS, 161, 154
Hunter, D. A., & Massey, P. 1990, AJ, 99, 846
Ivanov, V. D., Borissova, J., Pessev, P., Ivanov, G. R., & Kurtev, R. 2002, A&A, 394, L1
Ivanov, V. D., Borissova, J., Bresolin, F., & Pessev, P. 2005, A&A, 435, 107
Kleinmann, S. G., & Hall, D. N. B. 1986, ApJS, 62, 501
Koornneef, J. 1983, A&A, 128, 84
Lancon, A., & Rocca-Volmerange, B. 1992, A&AS, 96, 593
Luhman, K. L., Engelbracht, C. W., & Luhman, M. L. 1998, ApJ, 499, 799
Lumsden, S. L., & Puxley, P. J. 1996, MNRAS, 281, 493
Martín-Hernández, N. L., van der Hulst, J. M., & Tielens, A. G. G. M. 2003, A&A, 407, 957
Martins, F., & Plez, B. 2006, A&A, accepted
Messineo, M., Habing, H. J., Menten, K. M., et al. 2005, A&A, 435, 575
Meyer, M. R., Calvet, N., & Hillenbrand, L. A. 1997, AJ, 114, 288
Meyer, M. R., Edwards, S., Hinkle, K. H., & Strom, S. E. 1998, ApJ, 508, 397
Modigliani, A., Hummel, W., Abuter, R., et al. 2007, [arXiv:astro-ph/0701297]
Moffat, A. F. J., Jackson, P. D., & Fitzgerald, M. P. 1979, A&AS, 38, 197
Oliva, E., & Origlia, L. 1992, A&A, 254, 466
Panagia, N. 1973, AJ, 78, 929
Parker, Q. A., & Phillipps, S. 1998, PASA, 15, 28
Paumard, T., Genzel, R., Martins, F., et al. 2006, ApJ, 643, 1011
Pickles, A. J. 1998, PASP, 110, 863
Price, S. D., Egan, M. P., Carey, S. J., Mizuno, D. R., & Kuchar, T. A. 2001, AJ, 121, 2819
Repolust, T., Puls, J., Hanson, M. M., Kudritzki, R.-P., & Mokiem, M. R. 2005, A&A, 440, 261
Rousselot, P., Lidman, C., Cuby, J.-G., Moreels, G., & Monnet, G. 2000, A&A, 354, 1134
Russeil, D., Georgelin, Y. M., Georgelin, Y. P., Le Coarer, E., & Marcelin, M. 1995, A&AS, 114, 557
Schaller, G., Schaerer, D., Meynet, G., & Maeder, A. 1992, A&AS, 96, 269
Schreiber, J., Thatte, N., Eisenhauer, F., et al. 2004, in Astronomical Data Analysis Software and Systems (ADASS) XIII, ed. F. Ochsenbein, M. G. Allen, & D. Egret, ASP Conf. Ser., 314, 380
Scoville, N. Z., Hall, D. N. B., Ridgway, S. T., & Kleinmann, S. G. 1982, ApJ, 253, 136
Shepherd, D. S., & Churchwell, E. 1996, ApJ, 457, 267
Simon, M., Felli, M., Massi, M., Cassar, L., & Fischer, J. 1983, ApJ, 266, 623
Storey, P. J., & Hummer, D. G. 1995, MNRAS, 272, 41
Sugitani, K., & Ogura, K. 1994, ApJS, 92, 163
Sugitani, K., Tamura, M., & Ogura, K. 1995, ApJ, 455, L39
Thompson, M. A., Urquhart, J. S., & White, G. J. 2004, A&A, 415, 627
Urquhart, J. S., Thompson, M. A., Morgan, L. K., & White, G. J. 2004, A&A, 428, 723
Vacca, W. D., Garmany, C. D., & Shull, J. M. 1996, ApJ, 460, 914
Wainscoat, R. J., Cohen, M., Volk, K., Walker, H. J., & Schwartz, D. E. 1992, ApJS, 83, 111
Wood, D. O. S., & Churchwell, E. 1989a, ApJ, 340, 265
Wood, D. O. S., & Churchwell, E. 1989b, ApJS, 69, 831